İSTANBUL UNIVERSITY PRESS

Physics and Astronomy Reports
PAR 2025, 3 (2), 62–74
DOI: 10.26650/PAR.2025.00007

RESEARCH ARTICLE

Physical Properties of 29 March 2006 Solar Corona

H. Çakmak[1*]

[1]İstanbul University, Faculty of Science, Department of Computer Sciences, 34116, Beyazıt, İstanbul, Türkiye

ABSTRACT

On 29 March 2006, a total solar eclipse was observed in the Manavgat district of Antalya, Turkey. During the event, the solar corona was observed using an 8-inch mirrored telescope. White-light polarization observations were carried out at three distinct angles using a polarizing filter placed in front of the camera system. To calibrate the intensity of the roll film, photographs of the eclipse and the solar disk were taken with a traditional 35mm manual camera. Using the solar disk images obtained during the eclipse, an intensity calibration curve for the roll film was created. This curve was then used to calculate various physical properties of the solar corona, including intensity, degree of polarization, electron density, and mean temperature. The results of these calculations were compared with the corona models developed by van de Hulst (1950) and Saito (1970), as well as with findings from other researchers. Except for the degree of polarization, the measured physical parameters closely match the values given in the literature.

Keywords: Sun: corona – intensity – polarization, astrometry and celestial mechanics: eclipses

1. INTRODUCTION

The primary importance of total solar eclipses lies in the opportunity they provide to observe the solar corona during the brief period of totality. The solar corona is defined as the Sun's enigmatic outer atmosphere, which is characterized by its extreme faintness and is approximately one million times dimmer than the Sun's photosphere. This characteristic makes it challenging to observe directly, except during a solar eclipse. Despite its low particle density, the corona has an incredibly high temperature, reaching several million degrees. This paradox, along with to other unresolved questions, makes every total solar eclipse a valuable scientific event that draws significant attention. The corona's appearance, or morphology, suggests that its primary source of energy is the Sun's magnetic field. Changes in the strength and structure of the magnetic field, particularly between different phases of the solar cycle, affect the corona's visible shape. During the solar cycle's minimum phase, coronal structures tend to concentrate in the area near the Sun's equator. However, during the maximum phase, these structures exhibit a more even distribution across the entire solar disk. This finding suggests a close correlation between the shape and intensity of the solar corona and the activity of the sunspot cycle.

During the solar minimum, the corona's appearance is characterized by a nearly uniform intensity gradient extending from regions near the solar disk to more distant areas. This smooth gradient has made the development of a relatively simple model for minimum type corona possible, depending on the observed coronal intensity and the distance to the solar disk edge. The first model of the coronal intensity and polarization was developed by Schuster (1879), who provided the main solutions to all fundamental mathematical problems in this subject. Subsequently, Minnaert (1930) advanced the Schuster theory by including the limb-darkening effect of the solar disk, thereby enhancing its complexity and precision. Subsequently, the seminal works of Baumbach (1937, 1939) advanced this field by introducing the first general electron density function in a polynomial function with the form of r^{-n}, developed using white-light corona data obtained photometrically.

In the present day, the observation of total solar eclipses has a significant role in the verification of solar corona models. This is because they provide valuable insights into the general condition of the corona during any sunspot cycle. Following the detailed characterization of the general conditions in the solar corona for the minimum type of solar cycle, the variations from one solar cycle to another will be more effectively identified. This will provide an opportunity to specify the variations that have occurred during any sunspot cycle. Each solar corona exhibited during a total solar eclipse is characterized by distinct properties, which vary from one another to a certain extent. The total solar eclipse of 29 March 2006 occurred close to the time of the minimum phase of the 23rd solar cycle. This event is particularly significant, as it yielded further observational data for testing established corona models.

This study is an extensive review of the observational re-

Corresponding Author: H. Çakmak **E-mail:** hcakmak@istanbul.edu.tr
Submitted: 18.07.2025 • **Revision Requested:** 10.09.2025 • **Last Revision Received:** 28.09.2025 • **Accepted:** 08.10.2025 • **Published Online:** 18.11.2025

sults obtained for the 2006 eclipse. It is evident from the results obtained that the solar corona observed during this eclipse is consistent with the characteristics of the minimum type of corona. All physical parameters, with the exception of polarization, demonstrate a high degree of agreement with the models and numerous observational values as reported in the current literature. The instruments utilized for observation and data reduction are delineated in Section 2, while the stages of intensity calibration performed are explained in Section 3. The subsequent Section 4 presents the calculated values of total coronal ($K + F$) intensity and polarization degree, along with the K coronal intensity and its polarization degree P_K values. Furthermore, the results of electron density and average coronal temperature are given in Sections 5 and 6, respectively. Finally, a general discussion of the results of the eclipse is provided in Section 7.

2. OBSERVATION AND DATA REDUCTION

The solar corona was observed during the total solar eclipse on 29 March 2006, and this was conducted by the staff of the Astronomy and Space Sciences Department of Istanbul University in Ilıca, a town in the Manavgat district of Antalya, Turkey. The site of observation has coordinates of 31°22′ E and 36°49′ N, and an altitude of 42 meters. As illustrated in the upper panel of Figure 1, the observation location is proximate to the center line of the totality, about 650 m from the center line. Furthermore, certain circumstances associated with this eclipse are given in Table 1.

On the day of observation, weather conditions were favourable for the eclipse, with the sky being clear and free of clouds or fog. Consequently, multiple observations were conducted simultaneously at the observation site. Each observation had a specific purpose, and different types of equipment were used. The white-light polarization observation selected for this study was one of the observations made. The polarization observation was conducted using an 8-inch Meade brand mirrored telescope, which possesses a 203mm aperture and 1280mm focal length, with a classic 35mm manual camera attached to its focal point. A polarizing filter with a transmittance of 30% was utilized, which was then incorporated into an apparatus capable of rotation at three distinct angles 0°, 60°, and 120°, attached to the front of the camera.

Before observation, 25 photographs of the solar disk were

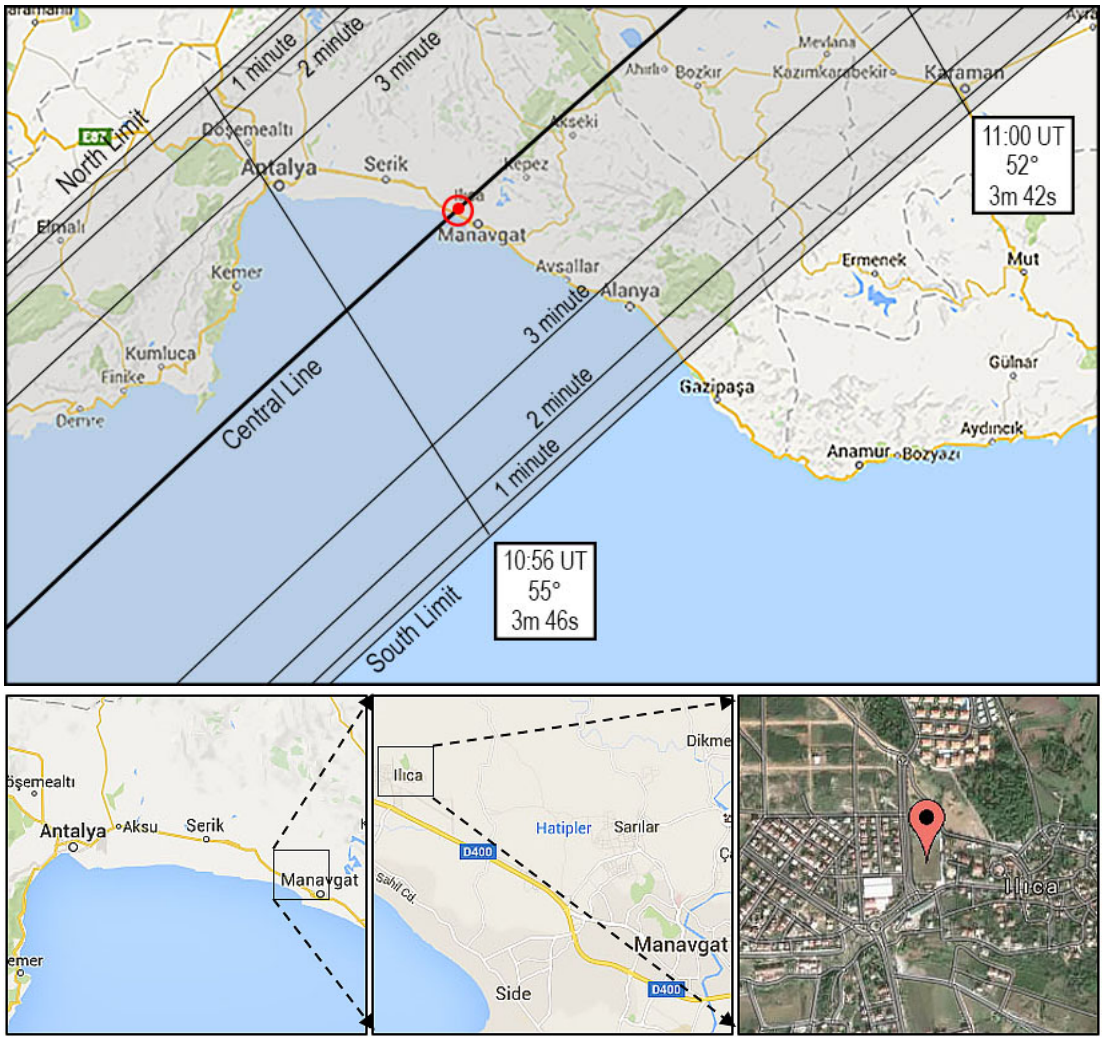

Figure 1. The upper panel illustrates the position of the total eclipse cone of 29 March 2000 over the southern part of Turkey. The location of the observation site is indicated by a small red point and a circle. This site is situated in close proximity to the central line of the eclipse. Furthermore, the location of the observation site at Ilıca city stadium is denoted by a small red location icon, as illustrated in the bottom-right image.

Table 1. Local circumstances of the March 29, 2006 eclipse at Ilıca site.

Eclipse parameters	
Beginning of totality	$10^h\ 55^m\ 02^s$ UT
End of totality	$10^h\ 58^m\ 47^s$ UT
Duration of totality	$3^m\ 45^s$
Width of totality	170 km
Altitude of the Sun during totality	from 56° to 44°
Ratio of the radii of apparent Sun and Moon	1.049
Position angle of second contact	47° from celestial N to E
Position angle of third contact	228° from celestial N to E
Parameters of the Sun's rotation axis and its equator	
Position angle, P (from celestial N to W)	- 26°.02
Equator angle, B_0 (latitude of apparent Sun's center)	- 6°.68

taken using a solar filter with a transmittance of 16×10^{-6} to calibrate the intensity response of the roll film used during the experiment. To avoid image saturation and ensure a broad dynamic range in the captured images, a combination of five diaphragm apertures with diameters of 95, 105, 115, 125, and 135mm was employed, along with five different exposure times (1/2, 1/4, 1/30, 1/60, and 1/125 seconds). An example set of these solar disk images, along with the corresponding diaphragm diameters, is presented in Figure 2. During totality, 36 photographs were taken over a period of 3^m45^s using a polarizing filter set at three different polarization angles. The same five exposure times used in the calibration shots were also applied during this phase. From this collection, 15 images were selected for the analysis of the solar corona's physical properties. The selected photographs, along with their respective exposure times and polarization angles, are shown in Figure 3.

As seen in Figure 3, the use of a wide-aperture telescope with 35mm film has resulted in an asymmetric space around the solar disk on the images, with the space on the polar regions being smaller than that on the equatorial regions. After the eclipse, the film was developed in the laboratory of the Department of Astronomy and Space Sciences, Faculty of Science, Istanbul University. All the eclipse and calibration images were then scanned into a computer using a Microtek Artix Scan 4000t Film Scanner, which features a 16-bit dynamic range, a pixel intensity range of 0 to 65535, and a 2000 DPI resolution.

3. INTENSITY CALIBRATION

Intensity calibration of the images utilized in the observational stage constitutes a crucial phase within the post-eclipse procedures. Despite the film manufacturer producing an intensity-exposure curve, this is frequently insufficient for the observation in question. It is well established that the intensity recorded in images varies with each eclipse observation. This is because the weather conditions and types of equipment used can have a significant impact on the results obtained. Consequently, the intensity-exposure curve of the images should be reformed for the current active observation. In the case of the 2006 eclipse, solar disk images captured with a solar filter were utilized to establish the "intensity calibration function" (ICF) of the images, using a novel approach previously developed. A comprehensive and detailed explanation of this topic can be found in Çakmak (2017). This article provides a concise overview of the procedures, introducing two key definitions. The first of these is the normalized intensity, I_N, which expresses any image intensity relative to the background intensity. This is given by

$$I_N = \frac{I_0}{I_{min}} \quad (1)$$

where I_0 is the intensity measured on the images and I_{min} is the lowest background intensity among all exposures taken. The second one, the relative intensity, I_R, is employed to express the observed intensity in the unit of average solar disk brightness. The efficacy of this parameter is dependent upon the equipment

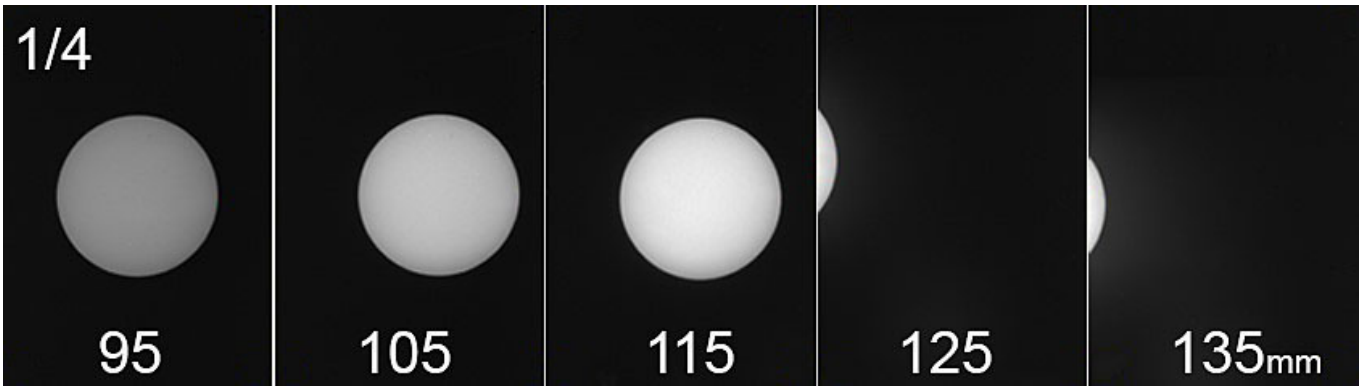

Figure 2. Here is an example of the solar disk images taken for intensity calibration at the 1/4 second exposure with five different diaphragm openings. In the last two images, most of the solar disk has been moved outside the frame to prevent excessive saturation of the sky background.

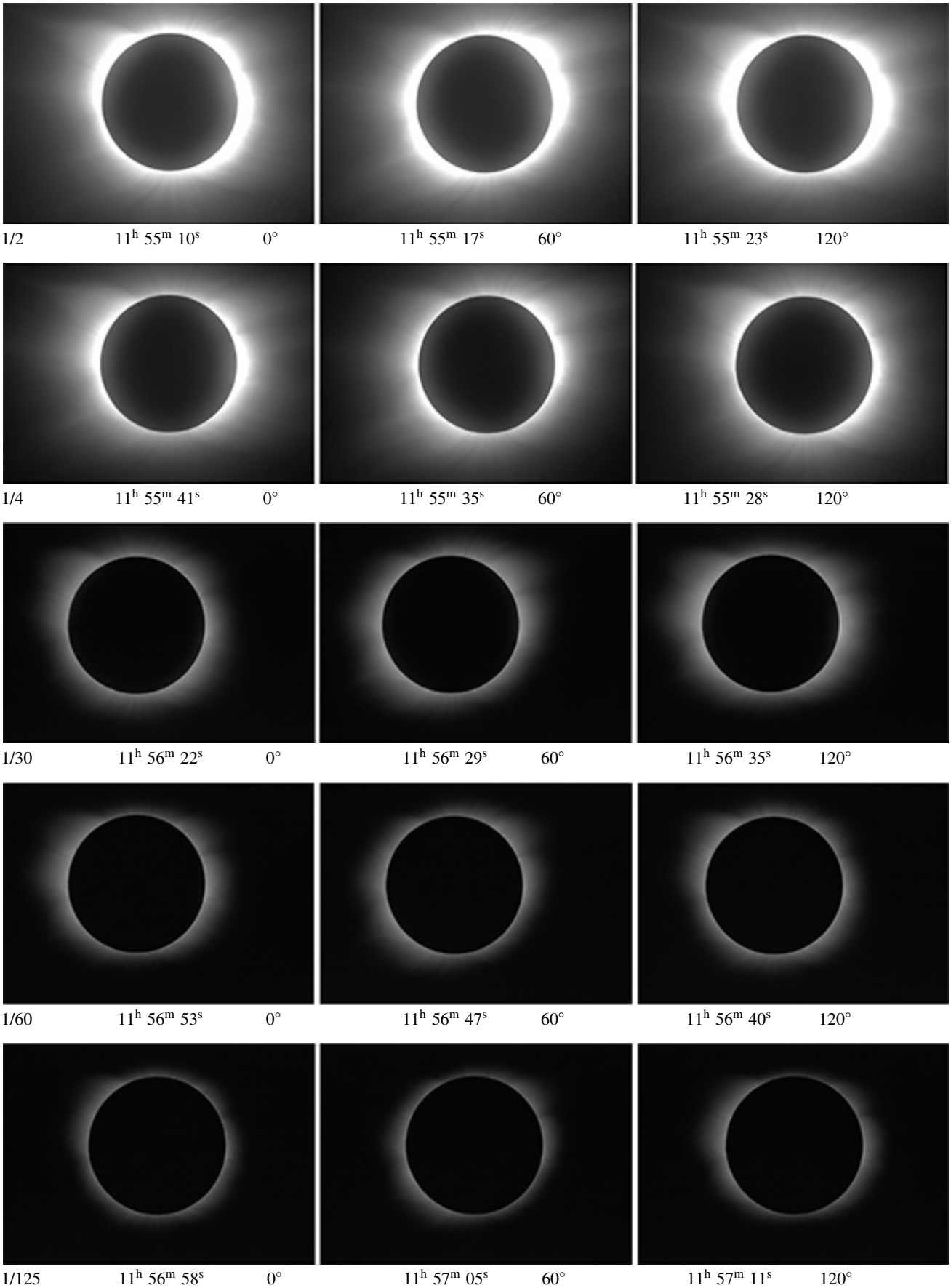

Figure 3. All the images of the eclipse that were utilized in the calculation process. The sequence of numbers from left to right on the bottom of the image corresponds to the exposure time, the time of observation, and the polarization angle, respectively.

utilized during observation, including the telescope aperture, the diaphragm, the transmittance of the polarize and solar filter, and the exposure time. In consideration of the assertions presented in the publications of McCluney (1994) and Arechhi & Koshel (2007), the relative intensity I_R can be expressed with the aforementioned parameters as,

$$I_R = \frac{I_{obs}}{I_\odot} = f_{int} * f_{pol} * t * \left(\frac{A_D}{A_O}\right) \quad (2)$$

where I_{obs} is the observed intensity. The quantity $I_\odot$ is average solar disk brightness, besides f_{int} and f_{pol} represent the transmittance of the solar filter and polarizer, respectively. The exposure time is denoted by t and the radii of the diaphragm opening and telescope aperture are indicated by A_D and A_O, respectively. The intensity calibration function (ICF) is then obtained by fitting an exponential curve, $y = A \times e^{Bx}$, to the graph relating I_N and I_R values.

As elucidated above, the mean intensity of each solar disk in the calibration images is measured as the mean intensity of a specific area over the disk that contains almost no saturated pixels. Due to the shifted disk images, in all images, the same region near the edge of the disk was selected for solar chromospheric disk brightness. Subsequently, the mean intensity of each calibration image is divided by the lowest background intensity observed across all exposures. The lowest value recorded was 5874. In addition, the transmittance of the solar filter and polarizer utilized in this eclipse observation is, respectively, 16×10^{-6} and 0.3. The calculated values of normalized and relative intensity are enumerated in Table 2, alongside the exposure times and diaphragms utilized. Figure 4 presents a graph between I_N and I_R values, with the curve fitted. The fitted curve function is obtained as

$$I_R = 5.7969 \times 10^{-9}\ e^{0.4979\, I_N} \quad (3)$$

with a correlation coefficient $R^2 = 0.97$. This function provides the relative intensity for a given normalized intensity on the images utilized in this eclipse.

After this step, the normalization process of the eclipse images is conducted by dividing the intensities of the solar corona by the lowest background intensity among all images of the eclipse. Subsequently, the relative intensity values for these normalized intensities of the corona in images are calculated by using the ICF given in Equation (3). Furthermore, it is important to note that another utility of this ICF is that the instrumental and sky contributions (I_{A+S}) to the total intensity can be found by taking the normalized intensity to be equal to 1 in Equation (3). This value ($I_N = 1$) is representative of the intensity of the sky itself. For this eclipse, this value is calculated as $0.95{\times}10^{-8} I_\odot$, which is relatively close to the value of $0.5{\times}10^{-8} I_\odot$ obtained by Kulijanishvili & Kapanadze (2005) during the eclipse of August 11, 1999. However, this value is slightly larger than the value of $0.2{\times}10^{-8} I_\odot$ obtained by Ney et al. (1961) during the eclipse on 2 October 1959.

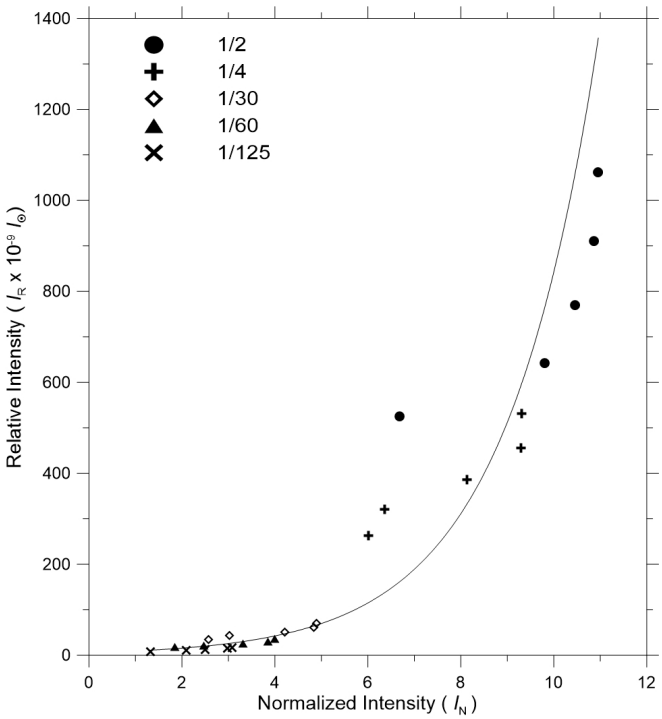

Figure 4. The intensity calibration curve acquired for the 2006 eclipse. Each exposure time is shown using a different symbol. The solid line represents the curve fitted.

4. BRIGHTNESS AND POLARIZATION

Before the calculations of brightness and polarization, it is necessary to create a composite image for each polarisation angle taken at five different exposure times that are 1/2, 1/4, 1/30, 1/60, and 1/125 seconds, respectively. The intensity in the composite image must be the average of the intensities taken in different exposures. Since there are five exposures, the sum of the intensity values must be divided by five. In addition, due to the linear correlation between intensity and exposure time, the total exposure times should also be taken into account in the intensity calculation (Çakmak 2017). In this observation, the composite intensity in each of the polarization angles (0°, 60°, 120°) is calculated using an empirical formula developed as

$$I_C = \frac{1}{\Sigma t_{exp}} \frac{I_{1/2} + I_{1/4} + I_{1/30} + I_{1/60} + I_{1/125}}{5} \quad (4)$$

where Σt_{exp} denotes the sum of selected exposure times in seconds and written as

$$1/2 + 1/4 + 1/30 + 1/60 + 1/125 = 0.808 \text{ second}$$

where $I_{1/2}$ denotes the measured intensity of the image exposed for 1/2 second, $I_{1/4}$ denotes exposure of 1/4 second, and so forth. Using the specific intensities at each polarization angle, the Stokes parameters for this eclipse were calculated as follows:

$$\begin{aligned} I &= \frac{2}{3}(I_0 + I_{60} + I_{120}) \\ Q &= \frac{2}{3}(2\, I_0 - I_{60} - I_{120}) \\ U &= \frac{2}{\sqrt{3}}(I_{60} - I_{120}), \quad V = 0 \end{aligned} \quad (5)$$

Table 2. Normalised and relative density values calculated using calibration images from the 2006 eclipse.

		Diameter of diaphragm opening in mm				
	Exposure (s)	95	105	115	125	135
Normalized Intensity	1/2	6.674	9.799	10.459	10.871	10.957
	1/4	6.016	6.364	8.132	9.292	9.314
	1/30	2.576	3.019	4.214	4.834	4.899
	1/60	1.853	2.472	3.315	3.850	3.996
	1/125	1.318	2.097	2.494	2.983	3.078
Relative Int. ($\times 10^{-9} I_{\odot}$)	1/2	525.613	642.093	770.220	909.995	1061.419
	1/4	262.807	321.046	385.110	454.998	530.709
	1/30	35.041	42.806	51.3480	60.666	70.761
	1/60	17.520	21.403	25.674	30.333	35.381
	1/125	8.410	10.273	12.323	14.560	16.983

where I is the total coronal brightness ($K + F$), Q is the amount of linear polarization in the vertical or horizontal plane, U is the value on +45° or −45° plane, and V is the amount of circular polarization which is assumed to be equal to zero in the eclipse observations (Billings 1966; Goldstein 2003). Subsequently, as expressed in Goldstein (2003), the degree of polarization, denoted P, and the angle of polarization, denoted by theta, are calculated for the total intensity by

$$P = \sqrt{Q^2 + U^2}$$
$$\theta = \frac{1}{2} \arctan\left(\frac{U}{Q}\right) \quad (6)$$

After subtracting the instrumental and sky contribution values I_{A+S} from the observed total coronal density, the total coronal density $K + F$ and polarization degree P_{K+F} values were calculated for the 2006 eclipse, and the resulting images are shown in Figures 5a and 5b, respectively. As illustrated in both figures, the selection of appropriate isolines for intensity and polarization degree was carefully performed. It is important to note that particular attention was paid to ensure that the selected isolines demonstrate the general gradient over a wide range and are equally spaced. The total corona intensities are calculated in all radial directions of polar angles between 0° and 360°, with 5° steps. As demonstrated in Table 3, the values of the four special polar angles (0°, 30°, 60°, and 90°) and the average total intensity values of the equatorial and polar regions are listed. In addition, the average polarization degree values of the equatorial and polar regions are also presented.

Figure 6 shows the intensity values separately for the polar angles of four specific directions, compared with the model values of Saito (1970) and the observational values of seven eclipses (Young 1911; Saito 1948; Ramberg 1951; Saito 1956; von Klüber 1958; Saito & Hata 1964; Waldmeier 1964). In the figure, the values for the 30° polar angle are shifted downward by one unit, those for 60° by two units, and those for 90° by three units, to improve visibility. Therefore, the numbers on the y-axis below -6 do not represent the true values for the polar angles of 30°, 60°, and 90°. As can be seen in Figure 6, the total intensity values obtained for the 2006 eclipse show quite good agreement with both the model and other observational values. Fluctuations in total coronal brightness with increasing

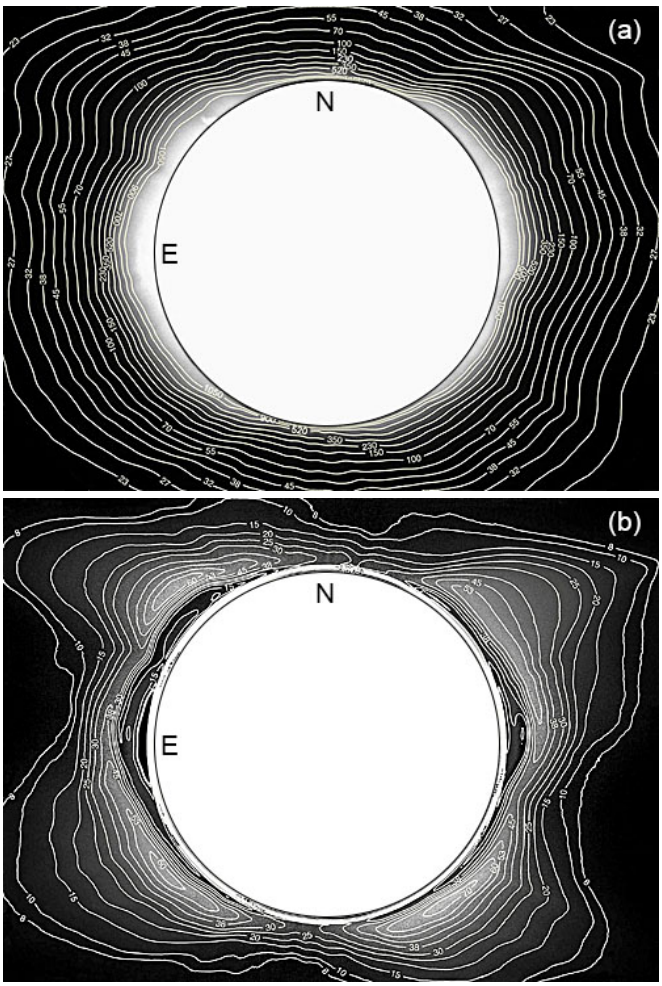

Figure 5. (a) Isophotes of total coronal brightness (numbers are in the unit of $10^{-9} I_{\odot}$) and (b) isolines of polarization degree (numbers are in percent) of the solar eclipse March 29, 2006.

distance from the disk are particularly evident at the 60° and 90° polar angles, and these are attributed primarily to asymmetries in coronal material distribution caused by magnetic activity variations over the solar cycle. Furthermore, this asymmetrical appearance is clearly visible in the polarization degree shown in Figure 5a. During the calculation of the average total brightness, the polar angles of 260°, 270°, 280°, and 310°, at which active coronal structures or regions exist, were not taken into

Table 3. Observational total coronal brightness $K+F$ and polarization degree (P_{K+F}) values of 29 March 2006 eclipse.

	$K+F$ corona ($\times 10^{-9} I_\odot$)						P_{K+F} (%)	
r ($R_\odot$)	0	30	60	90	Equ.	Pol.	Equ.	Pol.
1.10	510.9	891.0			1310.9	648.2	19.03	32.39
1.15	280.8	570.1	984.2		1046.3	364.2	26.73	36.30
1.20	166.4	308.7	732.2	983.5	781.8	200.5	36.44	33.17
1.25	110.6	174.9	468.1	701.2	513.2	128.1	44.69	25.95
1.30	81.2	118.2	265.4	432.4	292.8	91.0	46.12	19.57
1.35	64.4	86.6	172.6	251.6	180.2	70.1	39.79	15.00
1.40	53.8	66.9	125.8	159.6	125.4	57.2	32.40	13.87
1.45	45.9	53.9	97.7	111.8	94.0	48.1	26.81	12.28
1.50		45.1	78.8	84.6	74.3	42.3	22.47	11.56
1.55		39.3	65.8	67.9	61.2	37.7	19.40	10.67
1.60		34.7	56.6	56.2	52.0		17.11	
1.65		30.4	49.6	47.8	45.1		15.84	
1.70			44.0	41.7	39.9		14.61	

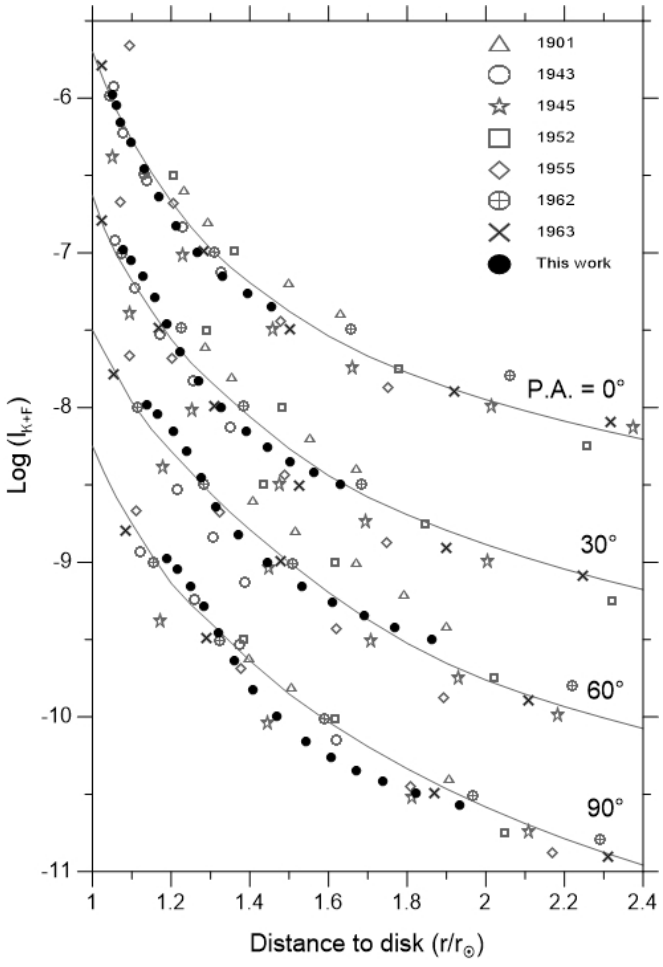

Figure 6. The average total coronal brightness of the solar eclipse on 29 March 2006 is shown at four specific polar angles, in comparison with the model values of Saito (1970) (straight line) and the observational values of seven eclipses (shown as symbols).

account to obtain a general intensity distribution and make a more appropriate comparison with the model values. This ensures spherical symmetry and an isotropic distribution of the observed intensity values.

The polarization degree P_{K+F} of the total coronal brightness of the 2006 eclipse is shown in Figure 7 in comparison with the model values of Saito (1970) and the results of the 25 February 1952 eclipse of von Klüber (1958). The 1952 eclipse occurred at a relatively similar stage of the solar cycle to that of the 2006 eclipse. The general trend of the polarization degree of this eclipse seems to be quite different from that of the model and other observations. But similar trends in the degree of polarization can also be seen in the results of observations made by Johnson (1934) at the eclipse on 14 February 1934, Fessenkoff (1935) at the eclipse on 21 August 1914, Dufay & Grouiller (1936) at the eclipse on 31 August 1932, Arnquist & Menzel (1970) at the eclipse on 12 November 1966, Koutchmy et al. (1978) at the eclipse on 30 June 1973 and Raju & Abhyankar (1986) at the eclipse on 16 February 1980.

A comparison of the obtained maximum values of polarization degree with Saito (1970) model values reveals the following conclusions. The maximum value of 46% in the equatorial region is reached at a distance of approximately $1.3R_\odot$, while the maximum value of the model in the equatorial region is 44% at a distance of $1.6R_\odot$. As can be seen from these values, both maxima are quite close to each other, but there is a $0.3R_\odot$ difference between the distances at which the maxima occur. The same situation is observed in the polar region. The maximum observational value is 36% at a distance of $1.17R_\odot$ while Saito (1970) model value is 25% at a distance of $1.16R_\odot$. Although the maximum distances of the model and observation are relatively close to each other, there is a significant difference of 11% between the two polarisation degrees. On the other hand, the maximum values of this observation appear to be close to the maximum values of von Klüber (1958) in both regions.

4.1. K coronal brightness and Its Polarization

Several methods are described in the literature for separating the K and F corona contributions to the total corona (van de Hulst 1950; von Klüber 1958; Ney et al. 1961; Koutchmy et al. 1978). In this study, the methods of von Klüber (1958) and Koutchmy et al. (1978) were applied separately. The F corona values obtained with these two methods were then compared with the F model values of van de Hulst (1950). However, as shown in Figure 8, the obtained F corona values for the

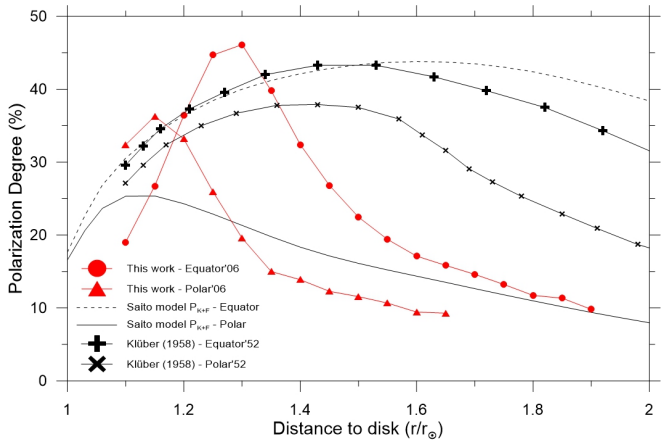

Figure 7. The polarization degree P_{K+F} of the solar eclipse on 29 March 2006 is compared with the model values of the polarization degree of Saito (1970) (the line with no symbol) and the observational results of von Klüber (1958).

2006 eclipse are not sufficiently satisfactory in comparison to the model values. In particular, the F corona values before a distance of $1.4R_\odot$ appear to be elevated and affected by the distribution of coronal matter formed by the present Solar Cycle. Therefore, a general approach was adopted, as explained below. The studies conducted by van de Hulst (1950), Saito et al. (1977), Morgan & Habbal (2007), and Hanaoka et al. (2012) provide evidence that the F corona remains relatively stable from cycle to cycle. This approach assumes that F coronal brightness, resulting from sunlight scattered by interplanetary dust, remains relatively stable. As a result, the model values of the F corona obtained from previous observations can be used in all other eclipse observations. Therefore, in this study, K coronal brightness of the 2006 eclipse is calculated by subtracting the F corona model values of van de Hulst (1950) from the observational total coronal $K + F$ brightness of this eclipse. The values of K coronal brightness obtained are presented in Table 4 for both the equatorial and polar regions. These values are also illustrated in Figure 9, which compares them with the model values of van de Hulst (1950) and Saito (1970).

The degree of polarization P_K of the K corona is calculated using the definition given in Koutchmy et al. (1978) as

$$P_K = \left(\frac{K+F}{K}\right) P_{K+F} \tag{7}$$

where $K + F$ and P_{K+F} are the total coronal brightness and its degree of polarization, respectively. The calculated polarization degree P_K values of the K corona are shown in Figure 10 in comparison with both equatorial and polar model values of van de Hulst (1950) and observational results obtained by several authors. The maximum value obtained for the equatorial region

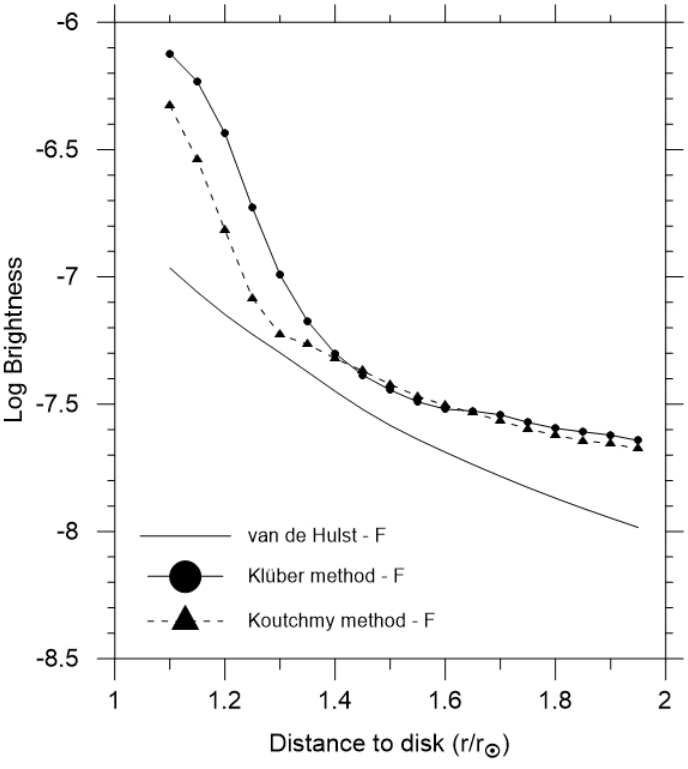

Figure 8. The observational F corona values obtained by two different methods are compared with the model values of van de Hulst (1950).

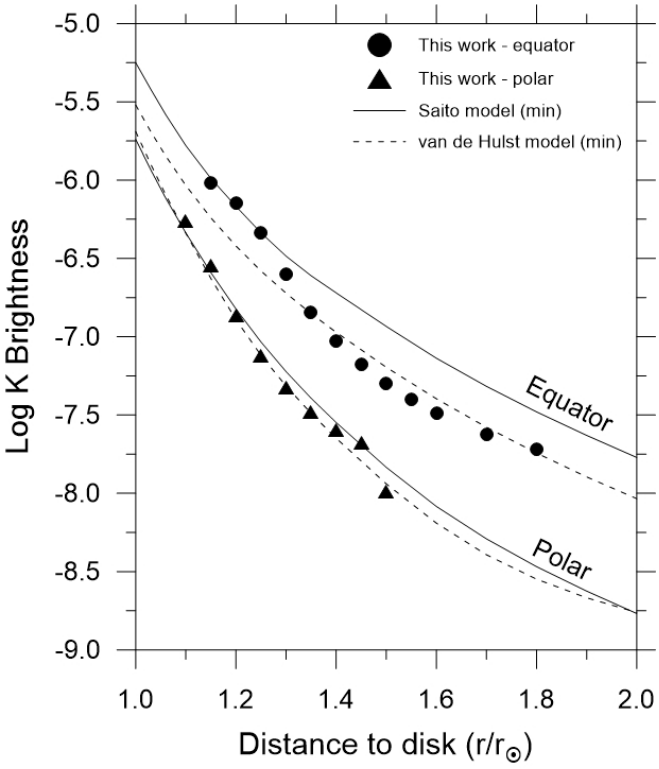

Figure 9. The K corona values of the 2006 eclipse compared with the models of van de Hulst (1950) and Saito (1970).

Table 4. The K coronal brightness values in $10^{-9} I_\odot$ unit for the equatorial and polar regions of the 2006 eclipse.

r ($R_\odot$)	Equatorial	Polar
1.10		547.8
1.15	965.7	284.9
1.20	716.2	136.8
1.25	459.9	75.6
1.30	249.1	47.1
1.35	143.9	32.9
1.40	93.9	25.2
1.45	66.4	21.0
1.50	49.9	10.3
1.55	39.5	
1.60	32.4	
1.70	23.9	
1.80	19.2	

is 55% at a distance of $1.3R_\odot$, and for the polar region, it is 42% at a distance of $1.15R_\odot$.

As seen in Figure 10, these maximum values of polarization degree are slightly higher than the other values. This discrepancy may result from asymmetries in coronal structure, which vary depending on the solar cycle phase. Such asymmetry can lead to an increased accumulation of coronal features at certain heliocentric distances. A sharp decline in polarization degree is also observed beyond the peak values. This rapid decrease is likely due to the absence of long-exposure images exceeding 1 second. In the present study, all exposures were shorter than 1 second, and the telescope used—featuring an 8-inch aperture—was relatively wide for this type of eclipse observation. Consequently, the solar coronal brightness may have been

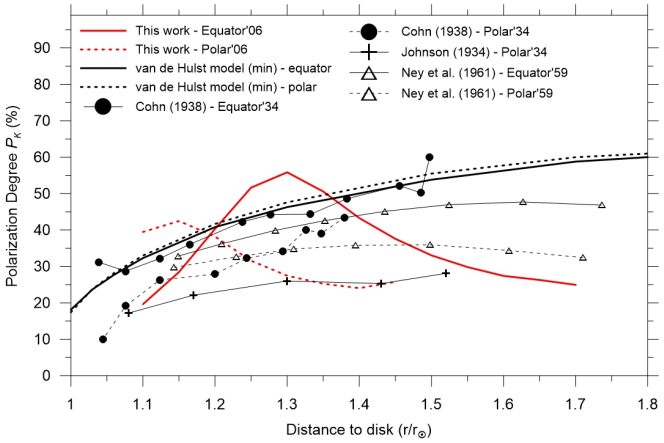

Figure 10. The polarization degree P_K values of the K corona (solid red lines) in comparison with the model values of van de Hulst (1950) (black solid lines) and observational results obtained by other authors (lines with symbol).

slightly overestimated at specific distances. This interpretation is also supported by the definition of the degree of polarization, which is given by

$$P_K = \frac{K_t - K_r}{K_t + K_r} = \frac{K_t - K_r}{K} \tag{8}$$

where K_t and K_r are the tangential and radial component of the K corona light, respectively (Schuster 1879; Baumbach 1939; van de Hulst 1950). According to this definition, the polarization degree is inversely proportional to the K coronal brightness. Therefore, an overestimation of coronal brightness leads to a lower calculated polarization degree. Had longer exposure times been employed, the average K-coronal brightness values would likely have been slightly lower. As a result, the polarization degree values beyond certain radial distances would have been more closely matched by the expected values.

5. ELECTRON DENSITY

According to existing corona models, K-corona light is produced by the scattering of free electrons. Therefore, the K coronal brightness is directly related to the number of electrons along the line of sight (von Klüber 1958; Kulijanishvili & Kapanadze 2005). With this perspective, van de Hulst (1950) has developed a method using successive approximations to calculate electron density using the observed K coronal brightness. With this approach, the author used the following equations;

$$K_t = \sum_s h_s\, x^{-s} = 1/2\,(1 + P_K)\,K \tag{9}$$

$$K_t - K_r = \sum_s k_s\, x^{-s} = P_K\,K \tag{10}$$

where $\sum_s h_s\, x^{-s}$ is a power series expressed as a three-element polynomial: $Ax^{-a} + Bx^{-b} + Cx^{-c}$. And other equations:

$$r\,C\,N(r)\,A(r) = \sum_s \frac{h_s}{a_{s-1}}\, r^{-s} = K_t(r) \tag{11}$$

$$r\,C\,N(r)\{A(r) - B(r)\} = \sum_s \frac{k_s}{a_{s+1}}\, r^{-s} = K_t(r) - K_r(r) \tag{12}$$

where a_s is a coefficient which calculated using gamma function given by author, C is a coefficient which equals to $3.44 \times 10^{-14}\mathrm{cm}^3$ and, A and B are the length of semi-major and semi-minor axis of the vibration ellipsoid, respectively (please refer to the article by van de Hulst (1950) to calculate A and B values as a function of a radial distance from the solar disk). The method developed by van de Hulst is somewhat difficult to apply, and many more attempts need to be made.

At this point, to simplify the calculations and reduce the number of iterations, the van de Hulst (1950) equations given in Equations (11 and 12) were mathematically rearranged from a different perspective, and a new calculation method was developed to obtain the corona electron density (for more information, see the article by Çakmak (2023)). According to this method, it is possible to define two different electron densities by

$$N_t(r) = \frac{f[K_t(r)]}{r\,C\,A(r)} \tag{13}$$

$$N_{t-r}(r) = \frac{f[K_t(r) - K_r(r)]}{r\,C\,\{A(r) - B(r)\}} \tag{14}$$

where $N_t(r)$ and $N_{t-r}(r)$ are the electron densities, and $f[K_t(r)]$ and $f[K_t(r) - K_r(r)]$ are the generated functions (GFs) for the $K_t(r)$ and $K_t(r) - K_r(r)$ components, respectively. Since the coronal density K is linearly proportional to the electron density $N(r)$, the relationship $K = 2\,K_t - (K_t - K_r)$ obtained from Equations (9 and 10) and valid between the corona components $K_t(r)$ and $K_t(r) - K_r(r)$ should also be valid for the electron density components. Therefore, the total electron density, $N(r)$, can be expressed similarly in terms of its components as follows:

$$N = 2\,N_t - N_{t-r} \tag{15}$$

Returning to the calculations, the K coronal brightness and polarisation degree P_K have been appropriately calculated up to this stage. Now, Equations (9 and 10) can be used to calculate the K corona components $K_t(r)$ and $K_t(r) - K_r(r)$ separately. By subsequently fitting $Ax^{-a} + Bx^{-b} + Cx^{-c}$ form polynomial curves to the values of these components, the coefficients s, h_s and k_s, as specified in Equations (9 and 10), can be obtained (see the article by Çakmak (2023) for details). After calculating the new coefficients h_s/a_{s-1} and k_s/a_{s+1} for each component of K_t and $K_t - K_r$ shown in Equations (11 and 12), the GFs are formed using these new coefficients by

$$\begin{aligned} f[K_t(r)] &= \sum_s \frac{h_s}{a_{s-1}}\, r^{-s} \\ f[K_t(r) - K_r(r)] &= \sum_s \frac{k_s}{a_{s+1}}\, r^{-s} \end{aligned} \tag{16}$$

The electron densities $N_t(r)$ and $N_{t-r}(r)$ of K_t and $K_t - K_r$ components are then calculated by using Equations (13 and 14). Finally, the total electron density required for the K coronal brightness is calculated by using Equation (15).

During the calculations, radial directions with polar angles between 260° and 280° and 315°, where active regions or powerful coronal streamers exist are not taken into account and

excluded from the computations. The calculated electron densities for the 2006 eclipse in both the equatorial and polar regions are listed in the rightmost column of Table 5, together with the other parameters used in the calculating process. These electron densities are also shown graphically in Figure 11 compared with the minimum corona model values of van de Hulst (1950) and Saito (1970) and the observational results of Allen (1973) and Newkirk (1967). As can be seen in Figure 11, the electron density values obtained for the 2006 eclipse are in good agreement with those of all others. However, when these values are compared with those of the models, the observed differences in electron density depending on the distance from the disk edge are interpreted as resulting from the asymmetric distribution of matter around the solar disk, which is specific to the 2006 eclipse.

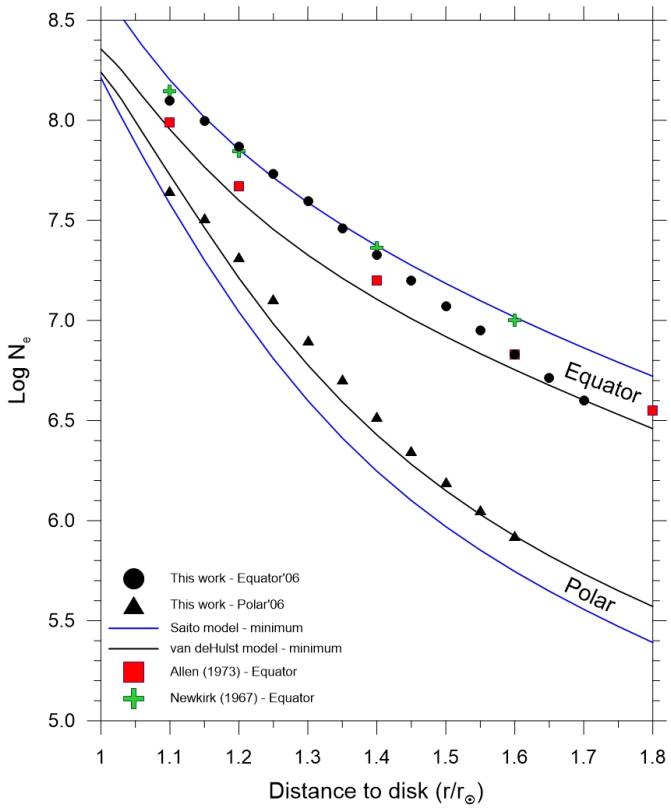

Figure 11. The electron density values for the 2006 eclipse compared with the minimum corona model values van de Hulst (1950) and Saito (1970) and several observational results.

6. AVERAGE CORONAL TEMPERATURE IN THE MID-HEIGHT

Informative data on the temperature in the corona can be obtained using the van de Hulst (1950) approach, which is based on the assumption of hydrostatic equilibrium in the coronal atmosphere. According to this approach, hydrostatic equilibrium is formed by the sum of the gravitational force per unit volume and the pressure gradient. This condition is expressed as

$$\mu\, m_{\rm H}\, \frac{G\, M_\odot\, N_{\rm e}}{(r\, R_\odot)^2} + k\, \frac{d(N_{\rm e}\, T)}{R_\odot\, dr} = 0 \qquad (17)$$

where G is the universal gravitational constant, $R_\odot$ is the solar radius, $M_\odot$ is the mass of the Sun, $N_{\rm e}$ is the number of the electrons per cm^3, μ is the mean molecular weight of the coronal gas, and is taken as 0.61 (Ney et al. 1961; Kulijanishvili & Kapanadze 2005) for this study, $m_{\rm H}$ is the mass of hydrogen atomic weight, r is the distance from the Sun's center in terms of the solar radius, k is the Stefan-Boltzmann constant and, T is the temperature (van de Hulst 1950). Rearranging this equation yields the following form:

$$\frac{T_1\, N_{\rm e}}{r^2} = -\frac{d(N_{\rm e}\, T)}{dr} \qquad (18)$$

where $T_1 = \mu\, m_{\rm H}\, G\, M_\odot / R_\odot\, k = 14.1 \times 10^6$ K. This equation can then be simplified to the form:

$$\frac{T_1}{T} = \frac{d}{d(1/r)} \ln N_{\rm e} + \frac{d}{d(1/r)} \ln T. \qquad (19)$$

In this equation, the first term denotes the gradient of electron density relative to distance, while the second term represents the temperature gradient. It is generally accepted that, under the assumption of hydrostatic equilibrium, this second term is negligible in the solar corona (van de Hulst 1950). Due to he gradient of temperature being negligible, with minor fluctuations occurring over comparatively brief distances within the corona, the determination of the temperature can be achieved from the gradient of the linear regression line ($\ln N_{\rm e}$ versus $1/r$) derived from the initial term of Equation (20) as

$$\frac{T_1}{T} = \frac{d}{d(1/r)} \ln N_{\rm e} \qquad (20)$$

The electron density versus $1/r$ plots for the 2006 eclipse in both the equatorial and polar regions are presented in Figure 12. As illustrated in the figure, the linear relationship predicted for an isothermal corona is not generally valid, and two distinct regions, designated as the near and far areas to the disk, are observed. After identifying areas showing a relatively linear slope in the electron density graph, the lines are adjusted to fit these areas. The temperatures of these regions are then derived from the slopes of the fitted lines, as described in Equation (20). The equations of the fitted lines for both the equatorial and polar regions of the 2006 eclipse are separately listed in Table 6 for the near (A_1, A_2) and far (B_1, B_2) areas of the disk, together with the calculated temperature values.

The temperature values calculated for the equatorial region during the 2006 eclipse were 1.82×10^6 K at a distance of $1.2R_\odot$ and 1.11×10^6 K at a distance of $1.5R_\odot$, and for the polar region, $1.15R_\odot$ and 0.82×10^6 K at a distance of $1.4R_\odot$, are slightly higher than the values obtained by both Ney et al. (1961) and Kulijanishvili & Kapanadze (2005). In the eclipse of 2 October 1959, Ney et al. (1961) obtained the temperature values as 1.22×10^6 K at a distance of $1.3R_\odot$ in the equatorial region, and 0.91×10^6 K at a distance of $1.8R_\odot$ in the polar region. In addition, during the eclipse of 11 August 1999, Kulijanishvili & Kapanadze (2005) obtained temperature values of 1.23×10^6 K at a distance of $1.3R_\odot$ in the equatorial region and 1.07×10^6 K at a distance of $1.8R_\odot$ in the polar region.

One potential explanation for the observed variations in the 2006 eclipse may be attributed to the 23rd Solar Cycle, which exhibited characteristics that differed from those of the preceding cycle. This cycle was characterised by an increased preva-

Table 5. The values used to calculate electron density (left side) and the results obtained for the 2006 eclipse (right side) are shown for both the equatorial and polar regions.

$r(r_\odot)$	K	P_K	$K_t - K_r$	K_t	$f(K_t - K_r)$	$f(K_t)$	N_{t-r}	N_t	N_e
A-equatorial region									
1.10	158.55	0.196	31.10	94.82	160.47	269.28	197.19	161.28	125.4
1.15	96.57	0.285	27.49	62.03	103.45	171.48	118.95	109.00	99.0
1.20	71.62	0.403	28.89	50.25	67.98	111.41	75.39	74.62	73.9
1.25	45.99	0.517	23.75	34.87	45.48	73.74	49.49	51.79	54.1
1.30	24.91	0.558	13.91	19.41	30.92	49.64	33.38	36.44	39.5
1.35	14.39	0.506	7.28	10.83	21.35	33.95	23.03	25.97	28.9
1.40	9.39	0.433	4.06	6.73	14.94	23.56	16.19	18.74	21.3
1.45	6.64	0.376	2.50	4.57	10.60	16.57	11.58	13.68	15.8
1.50	4.99	0.330	1.65	3.32	7.61	11.80	8.40	10.10	11.8
1.55	3.95	0.298	1.18	2.56	5.52	8.51	6.18	7.53	8.9
1.60	3.24	0.274	0.89	2.06	4.05	6.20	4.60	5.67	6.8
1.65	2.39	0.263	0.63	1.51	3.00	4.56	3.46	4.31	5.2
1.70	1.92	0.249	0.48	1.20	2.25	3.39	2.63	3.31	4.0
B-polar region									
1.10	54.78	0.395	21.63	38.20	76.47	115.36	93.97	69.09	44.2
1.15	28.49	0.425	12.10	20.30	35.99	58.04	41.39	36.89	32.4
1.20	13.68	0.382	5.22	9.45	18.31	30.60	20.30	20.49	20.7
1.25	7.56	0.316	2.39	4.97	10.05	16.90	10.93	11.87	12.8
1.30	4.71	0.275	1.29	3.00	5.92	9.78	6.39	7.18	8.0
1.35	3.29	0.252	0.83	2.06	3.71	5.92	4.00	4.53	5.1
1.40	2.52	0.240	0.61	1.56	2.45	3.74	2.65	2.98	3.3
1.45	2.10	0.258	0.54	1.32	1.68	2.46	1.84	2.03	2.2
1.50	1.03	0.287	0.29	0.66	1.19	1.68	1.32	1.44	1.6
1.55	0.50	0.266	0.13	0.32	0.87	1.18	0.97	1.05	1.1
1.60	0.34	0.264	0.09	0.22	0.64	0.86	0.73	0.79	0.8

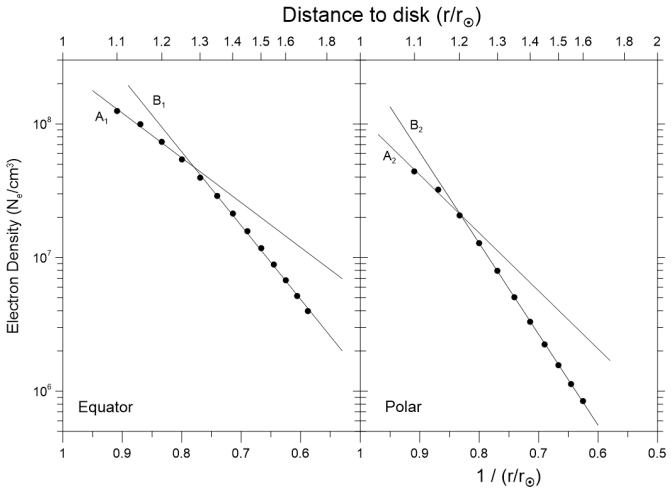

Figure 12. The graph of electron density gradient as a function of disk distance in the equatorial and polar regions. Solid lines indicate the range where a linear gradient occurs.

lence of sunspots with larger areas, the formation of brighter faculae and plage areas (De Toma et al. 2004; Kilcik et al. 2011b), and a higher frequency of coronal mass ejections (Kilcik et al. 2011a). In contrast, the obtained temperature values demonstrate a high degree of consistency with the values of van de Hulst (1950), which are reported to be 1.62×10^6 K in the equatorial region and 1.15×10^6 K in the polar region, for distances ranging from 1 to $3R_\odot$.

Table 6. The linear equations of the electron density gradient in the equator and polar region for the 2006 eclipse, and their mean distance and temperature values.

		Equations of the straight lines	$\langle r \rangle$ $(R_\odot)$	$\langle T \rangle$ $(\times10^6\mathrm{K})$
Equator	A_1	$\ln N_e = 7.71381 \times (1/r) + 11.66555$	1.2	1.82
	B_1	$\ln N_e = 12.70187 \times (1/r) + 7.77761$	1.5	1.11
Polar	A_2	$\ln N_e = 9.98710 \times (1/r) + 8.55229$	1.2	1.41
	B_2	$\ln N_e = 15.66973 \times (1/r) + 3.82678$	1.4	0.89

7. CONCLUSION

The physical parameters obtained from the 2006 eclipse are generally consistent with both the minimum corona model values of van de Hulst (1950) and Saito (1970) and some observational results in the literature. In particular, the total coronal $(K + F)$, and K brightness, electron density, and average coronal temperature values are in good agreement with the model values and those of others. However, such an agreement is not observed for the polarization degree values. As previously explained, the possible reasons for this phenomenon include the use of a relatively wide-aperture telescope and, more importantly, the absence of exposures longer than 1 second, as well as the asymmetric distribution of coronal brightness around the solar disk.

The fact that the results of the eclipse on 29 March 2006 are generally consistent with model values is primarily because

the 2006 eclipse occurred during the minimum period of the 23rd Solar Cycle, and the new method used in this observation is based on a correct approach. This consistency is also important for validating certain aspects of the existing models. For instance, the variation in brightness with distance is generally consistent with the model's predictions. However, it should be noted that these are not identical, and minor discrepancies may be observed, which vary from cycle to cycle depending on the activity of the Solar Cycle. The observed differences indicate that the matter in the corona does not have an isotropic distribution, as previously accepted by Ney et al. (1961). Consequently, it would be beneficial to consider modifying some of the approaches in current models for evaluation from a different perspective.

The method developed for the density calibration of roll films represents a novel approach in this field. Therefore, this phase of the study must be conducted with particular care. In this instance, images of the solar disk captured with filters and varying aperture sizes are employed to derive the density calibration function of the film utilised in the observational process. A careful examination of Figure 4 reveals that short exposure values are located in the lower left part of the curve, while long exposure values are located in the upper right part. The curvature is dependent on the exposure times used. Consequently, the range of exposure times used to construct this calibration curve must be carefully selected. A significant feature of this function is to provide the contributions of the sky and instrumental intensity ($I_A + I_S$) to the measured total intensity. In the context of film intensity measurements, intensity values are typically normalized relative to the background intensity, represented by the sky. Thus, a normalized intensity value of 1 corresponds to the sky's intensity, including any instrumental or additional contributions. Furthermore, it is important to note that the parameters used to create this function are observational parameters, including disk images, filters, exposure, and apertures. Accordingly, the density calibration function derived from these parameters can be considered an observational result.

The second method developed in this study is the direct calculation of electron density without using any approach method similar to those applied by van de Hulst (1950) and von Klüber (1958). The developed method may be regarded as a relatively practical and accessible alternative to existing approaches. As demonstrated in Figure 11, the observation of values that correspond to those of the model suggests that the developed method exhibits a comparatively precise approach. However, it is essential to consider a critical point regarding the method. In the process of polynomial curve fitting, it is important to ensure that the fitted curve passes through the general distribution of the observation points rather than passing close to each observation point. This is due to the presence of observational errors, which lead to deviations in the observed values.

While the results obtained for the 2006 eclipse are satisfactory, it would be beneficial to retest these new methods with other eclipse observations. Consequently, it would be valuable to establish contact with multiple researchers working on this subject in the future.

Peer Review: Externally peer-reviewed.

Author Contribution: Conception/Design of study - H.Ç.; Data Analysis/Interpretation - H.Ç.; Drafting Manuscript - H.Ç.; Critical Revision of Manuscript - H.Ç.; Final Approval and Accountability - H.Ç.

Conflict of Interest: Author declared no conflict of interest.

Financial Disclosure: This work was supported by the Istanbul University Scientific Research Projects Commission with project numbers 24242 and 470/27122005.,

Acknowledgements: Thanks to every staff member of the Department of Astronomy and Space Sciences who participated in the 2006 solar eclipse observation. Thanks to the anonymous referees for their valuable suggestions and comments, which significantly enhanced the manuscript.

Note: The Statistics Editor was not involved in the evaluation, peer-review and decision processes of the article. These processes were carried out by the Editor-in-Chief and the member editors of the editorial management board.

LIST OF AUTHOR ORCIDS

H. Çakmak https://orcid.org/0000-0002-1959-6049

REFERENCES

Allen C., 1973, Astrophysical Quantities 3rd ed.. Athlone Press, London

Arechhi A.V. Mesadi T., Koshel R., 2007, Field Guide to Illumination. SPIE field guides Vol. 11, SPIE

Arnquist W. N., Menzel D. H., 1970, Sol. Phys., 11, 82

Baumbach S., 1937, Astr. Nachr., 263, 121

Baumbach S., 1939, Astr. Nachr., 267, 273

Billings D., 1966, A Guide to the Solar Corona. Academic Press, New York

Çakmak H., 2017, Sol. Phys., 292, 186

Çakmak H., 2023, PAR, 1, 44

De Toma G., White O. R., Chapman G. A., Walton S. R., Preminger D. G., Cookson A. M., 2004, ApJ, 609, 1140

Dufay J., Grouiller H., 1936, Publications of the Observatoire de Lyon, 2, A129

Fessenkoff B., 1935, Russ. Astr. J., 12, 309

Goldstein D., 2003, Polarized Light Second Edition, Revised and Expanded. Marcel Dekker Inc, New York, Basel

Hanaoka Y., Kikuta Y., Nakazawa J., Ohnishi K., Shiota K., 2012, Sol. Phys., 279, 75

Johnson J. J., 1934, PASP, 46, 226

Kilcik A., Yurchyshyn V. B., Abramenko V., Goode P. R., Gopalswamy N., Ozguc A., Rozelot J. P., 2011a, ApJ, 727, 44

Kilcik A., Yurchyshyn V. B., Abramenko V., Goode P. R., Ozguc A., Rozelot J. P., Cao W., 2011b, ApJ, 731, 30

Koutchmy S., et al., 1978, A&A, 69, 35

Kulijanishvili V. I., Kapanadze N. G., 2005, Sol. Phys., 229, 45

McCluney W., 1994, Introduction to Radiometry and Photometry. Artech House Inc

Minnaert M., 1930, Z. Astrophys., 1, 209

Morgan H., Habbal S. R., 2007, A&A, 471, L47

Newkirk Gordon J., 1967, ARA&A, 5, 213

Ney E. P., Huch W. F., Kellogg P. J., Stein W., Gillett F., 1961, ApJ, 133, 616

Raju A. K., Abhyankar K. D., 1986, Bull. Astron. Soc. India, 14, 217

Ramberg J. M., 1951, Stockholms Observatoriums Annaler, 0016, 3.1

Saito K., 1948, Annals of the Tokyo Astronomical Observatory, 8, 63

Saito K., 1956, PASJ, 8, 126

Saito K., 1970, Annals of the Tokyo Astronomical Observatory, 12, 51

Saito K., Hata S., 1964, PASJ, 16, 240

Saito K., Poland A. I., Munro R. H., 1977, Sol. Phys., 55, 121

Schuster A., 1879, MNRAS, 40, 35

Waldmeier M., 1964, Z. Astrophys., 60, 28

Young R. K., 1911, Lick Observatory Bulletin, 205, 166

van de Hulst H. C., 1950, Bull. Astron. Inst. Netherlands, 11, 135

von Klüber H., 1958, MNRAS, 118, 201